Submitted Manuscript

Applied Spectroscopy

www.s-a-s.org

Azimuth Angle Dependence of Polarized Infrared Spectra of Injection-Molded Polyoxymethylene

Applied Spectroscopy
2024, Vol. 78(2) 197–208

DOI: 10.1177/00037028231217005
journals.sagepub.com/home/asp
Sage

Naoto Nagai

Abstract

Injection-molded polyoxymethylene (POM) has molecular chains mainly oriented in the injection direction. We investigated the directional dependence of the polarized infrared reflection and attenuated total reflection spectra by rotating the anisotropic POM sample. Because of the strong absorption and large frequency dispersion of the C–O vibration in the main-chain direction, we found phenomena such as shoulder wing generation that resulted from the mixing of optical responses attributed to the vibration in the main chain and that in the direction perpendicular to the main chain. The spectra of the directional dependence can be explained qualitatively because of the anisotropy of the mode with large frequency dispersion.

Keywords

Polyoxymethylene, infrared, IR, relative permittivity, reflection, attenuated total reflection, ATR, azimuth angle, frequency dispersion

Date received: 7 September 2023; accepted: 6 November 2023

Introduction

Polyoxymethylene (POM) is known as a plastic for engineering applications due to its excellent strength and impact resistance. Because of its simple molecular structure, POM has become an important material of research from a basic science perspective.[1–21]

Polyoxymethylene (POM) has a 9/5 or 29/16 helical trigonal crystal structure.[1,2] Moreover, POM is available in two types of mesostructures: extended-chain crystals and folded-chain crystals.[8–11] POM is characterized by its relatively high crystallinity compared to other plastics. Injection-molded POM generally exhibits a trigonal crystal structure and is composed of main chains distributed primarily along the mold flow from the gate injection port.[22,23] These structures are characterized by techniques such as infrared (IR) spectroscopy,[1–7] Raman spectroscopy,[4–14] and wide-angle X-ray scattering.[2,8–11,16,17]

However, difficulty in obtaining reproducibility has been reported for POM measured with powder methods such as KBr using IR.[3–5] This is believed to be caused by the strong coupling of the C–O bond vibration of the main chain with IR light, resulting in a surface phonon–polariton mode, combined with high crystallinity.[22–24] This mode strongly depends on the size and shape of the sample. Such vibrations are characterized by large frequency dispersion, namely the existence of regions where the real component of the relative permittivity (RP) is negative. Thus, a Reststrahlen band with high and wide reflection is observed in polarized reflection measurements in the injection direction. Our previous report showed that traces of this Reststrahlen band are also observed in the reflection spectra of the direction perpendicular to the injection.[25] Moreover, the in-plane distribution of the orientation angles of the main chain, characterized by Raman measurements, is bimodal, suggesting that the main chains are partially distributed along the transverse direction. Finally, the RPs in the main-chain direction and the direction perpendicular to the main chain were calculated in our previous report, using a two-phase model that simply adds the reflection of each other.[25] Nonetheless, the IR response obtained by mixing the main chains and those perpendicular to the main chains was hard to explain by the effective medium theory (EMT).

On the other hand, when measuring injection-molded POM using the attenuated total reflection (ATR) method, a shoulder wing appears in the 1000–950 cm^{-1} region.[23] Although this region is very close to the range where the real component of the RP in the main-chain direction becomes negative, it is

Graduate School of Science and Technology, Niigata University, Nishi-ku, Niigata, Japan

Corresponding Author:
Naoto Nagai, Graduate School of Science and Technology, Niigata University, 8050 Ikarashi 2 no-cho, Nishi-ku, Niigata 950-2181, Japan.
Email: nnagai@gs.niigata-u.ac.jp

generally not immediately associated with the occurrence of the shoulder in ATR spectra, as can be seen from the isotropic spectral calculations. Devlin et al.[26] reported spectra with similar shoulders in the frequency dispersion region of the large 1300 cm^{-1} mode obtained from *p*-polarized ATR spectra of nitrate crystals grown with the trigonal axis perpendicular to the prism plane (shoulders were not observed in *s*-polarized ATR spectra). This result suggests that the ATR optical response of uniaxial substances with large frequency dispersion may cause the apparent band because of anisotropy. To investigate the origin of the shoulder observed in the ATR spectrum of POM, polarized spectra with varying main-chain azimuth angles should be studied. The azimuthal dependence of IR spectroscopy is used to determine the detailed arrangement of the molecules.[27,28] However, this analysis is generally conducted for modes with small-frequency dispersion. If anisotropy from the modes with large frequency dispersion causes shifts or new peaks to appear, as shown in Devlin et al. examples, errors in band assignment and structural analysis may occur. In general, polymeric materials do not often exhibit such a substantial frequency dispersion. However, we have previously identified substances such as polytetrafluoroethylene and polyglycolic acid as materials where the real component of the RP becomes negative. Polyethylene oxide is also a candidate where the real part of RP becomes negative.[12] Furthermore, we have shown that phenomena where the frequency dispersion increases can occur with mechanical processes such as stretching or extrusion, as well as during heat treatment of POM.[23–25] These phenomena, coupled with the crystalline nature of polymers, indicate that the above-mentioned occurrences are not necessarily unique. Therefore, it is crucial to clarify the physical characteristics of the spectra, such as the azimuthal dependence of modes with large frequency dispersion, before performing a detailed chemical structural analysis.

Previous studies on the azimuthal dependence of modes with large frequency dispersion have generally been conducted with the perspective of using these modes as optical devices based on reflection.[29] Regarding the optical response of uniaxial crystals, such as their transmission and reflection, Yeh[30] provided theoretical equations and reported examples of their application to optical filters and other devices. Unfortunately, no examples of their application to spectroscopy have been provided. Because their equations involve no approximations, these equations are expected to be applicable even to the modes with large frequency dispersion. As far as we know, there are no examples of theoretical spectrum reproduction of the azimuth angle dependence using the RP of uniaxial crystals with very large frequency dispersion. When analyzing the azimuthal dependence of POM, the bimodality phenomenon mentioned before should be considered. Hereafter, we refer to the direction perpendicular to the main chain of the molecules as "orthogonal".

In this study, we determined the RPs of the main-chain direction and the orthogonal direction, using the reflection spectra of POM, with a particular focus on the bimodal phenomenon. Then, we checked whether the azimuthal dependence of the reflection spectra could be explained through Yeh's equation derived from these RPs. Finally, we verified whether the azimuthal dependence of the ATR spectra could be explained by the same RPs, with the aim of understanding the characteristics of the optical response of anisotropic crystals with large frequency dispersion.

Experimental

Materials and Methods

The POM resin was DuPont Delrin 500P NC010, which has a molecular weight (M_w) of approximately 60 000 g/mol. The injection-molding sample was prepared at 190 °C and a filling speed of 50 mm/s. And an $89 \times 49 \times 2$ mm molding plate was obtained. The gate is located at the center of the 49 mm side. A 15×15 mm sample was cut from the central portion of this plate and was provided for measurements.

Optical Setup

The injection-molded POM is an anisotropic material, and its main chains are mainly oriented along the molding flow on the sample surface. Figure 1 shows the optical setup for the measurements. Taking the *x*,*y*,*z* axes as the spatial coordinate system, the *x*,*y*-plane is on the sample surface and the *z*-axis is perpendicular to the sample surface. On the other hand, if representing the orientation axes of POM as *a, b, and c*, with *c* as the axis of the main-chain direction (injection

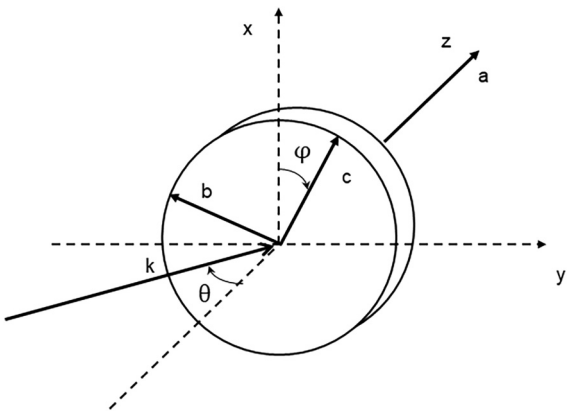

Figure 1. Optical setup for measurements and calculations. The letters *x*, *y*, and *z* represent the coordinate axes in space. The sample surface is assumed to be on the *x*,*y*-plane. The letters *a*, *b*, and *c* represent the crystal axes of a uniaxial sample. The main-chain direction is assumed to be along the *c*-axis, and the orthogonal directions are along the *a*-axis and *b*-axis. The light is assumed to be incident at an angle of θ with the *k*-vector direction (in the *y*,*z*-plane). The azimuth angle is φ. Our sample is supposed to be composed of main chains *c* distributed mainly along the *x*-direction, partially along the *y*-direction (bimodality), but not in the *z*-direction, when $\varphi = 0°$.

direction), *a* and *b* become the axes of the orthogonal (transverse) directions (without considering bimodality). Now, assuming the light enters at an incident angle of θ from the direction of vector k in the *y*,*z*-plane, let the azimuth angle φ be the angle from the *x*-axis to the main-chain *c*-axis. Hereafter, we assume that the main chains are distributed in the *x*,*y*-plane, and not in the *z*-direction. In other words, we assume that there are no molecular chain components that are inclined in the *z*-direction or aligned to the *z*-direction. If the incident light is *s*-polarized at $\varphi = 0°$, the reflected light becomes the optical response in the main-chain direction, while the *p*-polarized light becomes the optical response in the orthogonal direction plane (the *a*, *b*-plane). When the incident light is *s*-polarized at $\varphi = 90°$, the reflection becomes the optical response in the *b*-axis (the orthogonal direction). For *p*-polarized light at $\varphi = 90°$, the reflection becomes the optical response in the *c*, *a*-plane, where the main-chain and orthogonal direction are mixed.

Infrared (IR) Spectroscopy

Infrared (IR) spectra were recorded using a Nicolet 6700 (Thermo Fisher) Fourier transform (FT) IR spectrometer equipped with a Seagull attachment with a wire-grid polarizer. The beam diameter at the sample surface was approximately 1 mm. A deuterated triglycine sulfate (DTGS) detector was used, and the resolution was 4 cm^{-1} with 16 accumulations. The angle of incidence (θ) was set to 23° for the measurements. This angle should be smaller, but we set this value for comparison with the spectral shapes from our previous microscopic specular reflectance measurements.[22–25] The polarizer was placed in front of the detector after the beam was reflected off the sample surface, and *s*- and *p*-polarized measurements were conducted. We performed azimuth-angle-dependent reflectivity measurements by rotating the sample.

The ATR measurements were collected using a Spotlight (PerkinElmer) instrument equipped with an ATR attachment from PIKE Technologies with an ATR prism of germanium (Ge) at a fixed incident angle of 45° and a wire-grid-type polarizer built on a KRS-5 substrate. A DTGS detector was used in the measurements; the resolution was 4 cm^{-1} with 16 accumulations. The azimuth-angle-dependent ATR spectra were obtained by rotating the sample as was done in the reflectivity measurements.

When the azimuth angle is $0° < \varphi < 90°$, the component converted from the *s*-polarized wave to the *p*-polarized wave in the process of reflection and ATR, and the component converted from the *p*-polarized wave to the *s*-polarized wave may appear. Therefore, in addition to the polarized measurements mentioned above, reflection and ATR measurements with two polarizers were also performed by inserting another polarizer on the incident side before reflection.

To investigate the change in the spectral shape produced by the degree of contact between the sample surface and the ATR prism, we conducted measurements by gradually releasing the sample-pressing rod, although the gap thicknesses were unknown. These measurements were performed with *p*-polarized light at $\varphi = 90°$.

Results

Reflection Spectra

Injection-molded POM typically exhibits a tendency for the main chains to be aligned parallel to the direction of injection.[22,23] However, the results from in-plane orientation distribution analysis by Raman spectroscopy in a previous report showed a slight transverse alignment to the injection direction, namely, a bimodal distribution.[25] This indicates a structure in which main-chain orientation components are mixed with those of the orthogonal direction. Similar mixing also occurs in the transverse direction. As shown in the solid lines in Figure S1 (Supplemental Material), polariton reflection from the main-chain direction is mixed at slightly lower positions from 1000 cm^{-1} in the transverse direction at $\varphi = 90°$ in the *s*-polarized reflection spectra. Likewise, the E_1 mode derived from the orthogonal vibration from C–O–C symmetric stretching is mixed at approximately 930 cm^{-1} in the injection direction at $\varphi = 0°$ in the reflection spectrum.[12,23] As described in our previous report, the mixing ratios of each cross-component and the pure RPs in the main-chain and orthogonal directions were determined by performing least square fitting to the reflection spectra at $\varphi = 0°$ and $\varphi = 90°$.[25]

The results of the simultaneous calculation of the reflection spectra at $\varphi = 0°$ and $\varphi = 90°$ are shown by the dotted lines in Figure S1 (Supplemental Material), which proves that using a two-phase model can better explain the data on the mixing ratio of each cross-components than using the EMT. For our sample, the mixing ratio was 17.8% for each orientation direction (this was slightly lower than for the previously reported sample, which was possibly due to the different sampling positions). Figure 2 displays the RP of the main-chain direction and the orthogonal direction, obtained by spectral fitting. Here, both $\varphi = 0°$ and $\varphi = 90°$ were simultaneously calculated. In other words, the mathematically obtained spectra in Figure 2 remove the main chain or orthogonal contribution of the $\varphi = 90°$ and 0° spectra, respectively. As previously described, a negative region exists in the real component of the RP in the ranges of 992–915 cm^{-1} and 1132–1105 cm^{-1} in the main-chain direction, and in the range of 942–935 cm^{-1} in the orthogonal direction. Figure S2 (Supplemental Material) shows the complex refractive index (CRI) of the main-chain and orthogonal directions.

The solid lines in Figure 3 show the experimental results of the azimuthal dependence of the reflection spectra for *s*-

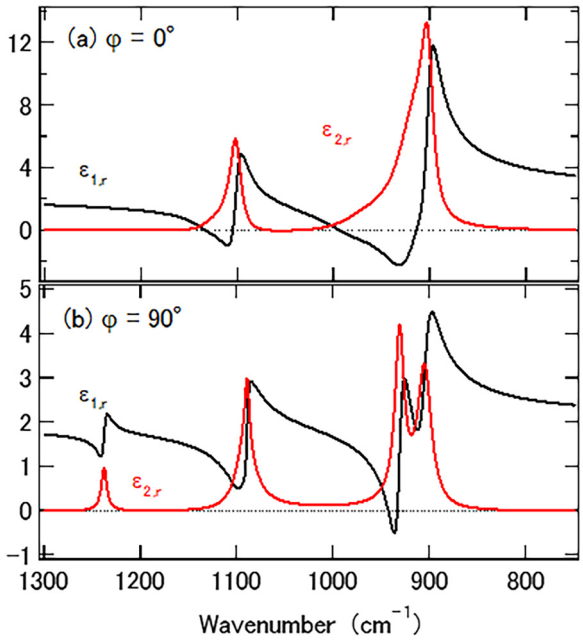

Figure 2. (a) The RP of the main-chain direction ($\varphi = 0°$), and (b) the RP of the orthogonal direction ($\varphi = 90°$), calculated from the s-polarized reflection spectra.

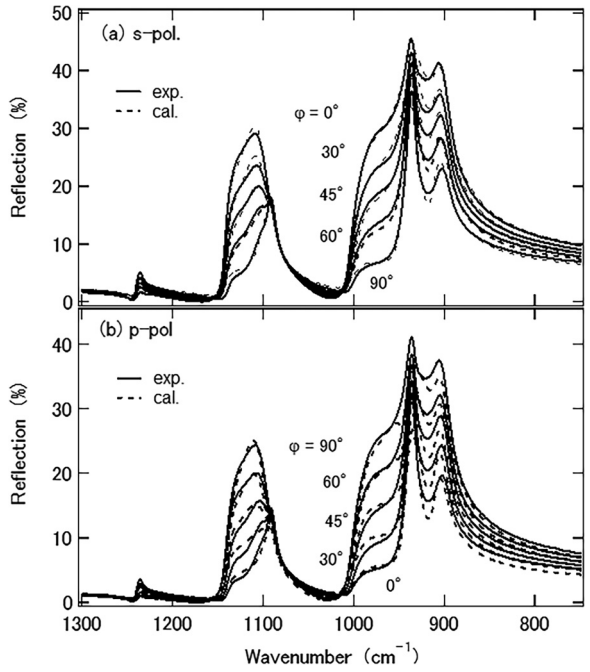

Figure 3. Azimuth angle dependence of the polarized reflection spectra of injection-molded POM (solid line) and the calculated reflection spectra using the RP of Figure 2 or the CRI of Figure S2 (Supplemental Material) on the two-phase model (dotted line): (a) s-polarization and (b) *p*-polarization.

and *p*-polarization. To interpret these azimuthal-dependent spectra using the RP of the main-chain and orthogonal direction in Figure 2 or the CRI (Figure S2, Supplemental Material), two factors should be considered: (i) the optical response of the anisotropic medium and (ii) the mixing of the cross-components.

(i). *Optical Response of Anisotropic Media*

For *p*-polarization at $\varphi = 90°$, the optical response should be calculated as an anisotropic medium considering the RP of the main chain and orthogonal component, whereas, for *p*-polarization at $\varphi = 0°$, the optical response should be calculated as an isotropic medium composed only of the orthogonal component. For *s*-polarization at $\varphi = 0°$, the optical response reflects from the main-chain direction, and for *p*-polarization at $\varphi = 0°$, it reflects from the orthogonal direction. For *s*-polarization with $0° < \varphi < 90°$, the optical response is expected to correspond to an anisotropic medium, considering the RPs of the main-chain and orthogonal directions. Hence, the sample should be treated as an anisotropic medium to calculate the response with respect to the azimuth angle.

In these experiments, the polarizer is set after the light is reflected on the sample surface. That is, when the light enters the sample, the light is a mixture of *s*- and *p*-polarizations (unpolarized), but the reflected light is polarized after passing through the polarizer. In the case of isotropic media, the reflected light is *s*-polarized when the incident light is *s*-polarized (R_{ss}) and *p*-polarized when the incident light is *p*-polarized (R_{pp}). However, for substances with in-plane anisotropy, coupling occurs between *s*-polarization and *p*-polarization for $0° < \varphi < 90°$. This implies that some components are converted from *s*-polarized incident waves to *p*-polarized waves after reflection on the sample surface (R_{sp}), whereas other components are converted from *p*-polarized incident waves to *s*-polarized waves after reflection on the sample surface (R_{ps}). Therefore, in these polarizer arrangement experiments, $R_{ss} + R_{ps}$ is observed when aligned with the *s*-polarization, and $R_{pp} + R_{sp}$ is observed when aligned with the *p*-polarization. Note that $R_{sp} = R_{ps} = 0$ when the azimuth angle φ is 0° or 90°.

The IR spectrum changes that are dependent on the azimuth angle can be calculated using Yeh's equation,[30] considering the CRI $n(\nu)$ and $k(\nu)$, where ν is the frequency. Yeh's equation can be modified and eventually takes the following form:

$$A = n_{bz}(n_z + n_{bz}) \sin\varphi \tag{1}$$

$$B = n_b^2(n_z + n_{cz}) \cos\varphi \tag{2}$$

$$C = -\left(nn_{bz} + \frac{n_z(\beta^2 + n_{bz}^2)}{n}\right) \cos\varphi \tag{3}$$

$$D = \left(nn_{bz}^2 + \frac{n_z n_{cz}(\beta^2 + n_{bz}^2)}{n}\right) \sin\varphi \tag{4}$$

$$A' = n_{bz}(n_z - n_{bz}) \sin\varphi \quad (5)$$

$$B' = n_b^2(n_z - n_{cz}) \cos\varphi \quad (6)$$

$$C' = -\left(nn_{bz} - \frac{n_z(\beta^2 + n_{bz}^2)}{n}\right) \cos\varphi \quad (7)$$

$$D' = \left(nn_{bz}^2 - \frac{n_z n_{cz}(\beta^2 + n_{bz}^2)}{n}\right) \sin\varphi \quad (8)$$

$$r_{ss} = \frac{A'D - B'C}{AD - BC} \quad (9)$$

$$r_{ps} = \frac{AB' - A'B}{AD - BC} \quad (10)$$

$$r_{sp} = -\frac{CD' - C'D}{AD - BC} \quad (11)$$

$$r_{pp} = \frac{AD' - BC'}{AD - BC} \quad (12)$$

$$R_s = |r_{ss}|^2 + |r_{ps}|^2 \ (= R_{ss} + R_{ps}) \quad (13)$$

$$R_p = |r_{pp}|^2 + |r_{sp}|^2 \ (= R_{pp} + R_{sp}) \quad (14)$$

Here, we used the following notations: $\beta = n \sin\theta$, $n_z = n\cos\theta$, $n_{bz}^2 = n_b^2 - \beta^2$, $n_{cz}^2 = n_c^2 - \beta^2[\cos^2\varphi + (n_c^2 / n_b^2)\sin^2\varphi]$. As shown in Figure 1, the incident vector is taken in the y, z-plane, n is the refractive index of the incident medium, θ is the incident angle, n_c is the CRI in the main-chain direction, and n_b is the CRI in the orthogonal direction.

We used $\theta = 23°$ and $n = 1$ for the calculations. Two solutions (plus and minus) appear for n_{bz} and n_{cz} depending on the incidence angle, azimuth angle, and frequency dispersion. However, it is not obvious which solution is physically meaningful. Thus, to select a physically meaningful solution, we correct for the π-jumps in phase by adding the πlterm with $l = \pm 1$ so that we obtain the smooth reflection (or ATR) spectra.

$$n_{bz} = \pm\sqrt{n_b^2 - \beta^2} \quad (15)$$

$$= |n_{bz}| \exp\left(i\tan^{-1}\{[\mathrm{Im}(n_{bz})/\mathrm{Re}(n_{bz})] \pm \pi l\}\right) \quad (16)$$

$$n_{cz} = \pm\sqrt{n_c^2 - \beta^2\left(\cos^2\varphi + \frac{n_c^2}{n_b^2}\sin^2\varphi\right)} \quad (17)$$

$$= |n_{cz}| \exp\left(i\tan^{-1}\{[\mathrm{Im}(n_{cz})/\mathrm{Re}(n_{cz})] \pm \pi l\}\right) \quad (18)$$

(ii) *Mixing of Cross-Components (Bimodal Effect)*

To determine the reflectance of the injection-molding direction, the mixing ratio was set to 82.2–17.8% for the main-chain-orthogonal direction reflection in a two-phase model. Likewise, for the reflectance of the transverse direction, the mixing ratio was set to 82.2–17.8% for the orthogonal-main-chain direction reflection. Assuming that the cross-components are mixed in the same ratio for other azimuth angles, the reflection spectra that result from the mixing effect can be calculated for both the *s*- and *p*-polarization. For example, the reflection of the cross-component of an azimuth angle of 30° is equivalent to the reflection of an azimuth angle of 60°, In the same way, the reflection of the cross-component of an azimuth angle of φ is equivalent to the reflection of an azimuth angle of 90° - φ.

The reflection spectra are shown as the dotted lines in Figure 3. The azimuthal dependence of the *s*-polarized spectra agrees with the experiments. Although the *p*-polarized spectra are slightly less consistent compared to the *s*-polarized spectra, they still explain the shoulder shapes of the Reststrahlen band near 1000 and 1130 cm^{-1} fairly well, even though only the RP determined using the *s*-polarized spectra were employed. Therefore, Yeh's equation is effective in verifying the azimuthal dependence of the IR reflection spectrum of in-plane oriented samples.

Attenuated Total Reflection (ATR) Spectra

Figure 4 shows the experimental results of the azimuthal dependence of the ATR spectra. Let us momentarily neglect the bimodal effect. For *s*-polarization at $\varphi = 0°$, the ATR spectrum should represent the main-chain direction, whereas for *p*-polarization at $\varphi = 0°$, both in-plane and depth directions consist of orthogonal components. Thus, the ATR spectrum should behave isotropically with respect to only the orthogonal component. At $\varphi = 90°$, the ATR spectrum for *s*-polarization should represent the orthogonal direction, whereas, for *p*-polarization, it should represent the main-chain component in the in-plane direction and the orthogonal component in the depth direction, thus forming an anisotropic ATR spectrum. Because ATR spectra generally strongly reflect the shape of absorption, they correspond well to the imaginary component of the RP shown in Figure 2. However, the shoulders at 1000–950 and 1130–1100 cm^{-1} appearing in the ATR spectra cannot be explained only by the large frequency dispersion when the material is supposed to be isotropic, as they are not present in the imaginary component of the RP (Figure 2b).

The IR spectra of POM reveal its anisotropy and very large frequency dispersion that results in a polariton mode. Therefore, we examined the effect of anisotropy in terms of the azimuthal variation of the ATR spectra when the degree of frequency dispersion changed using several Lorentz model spectra (see the Appendix for details). The anisotropic mode peaks of both the main-chain and orthogonal directions are just added as the azimuth angle changes to Lorentz modes with small absorption and small-frequency dispersion (Figure S4, Supplemental Material). However, for modes with large absorption intensity and large frequency dispersion, which exhibit a negative RP, various optical

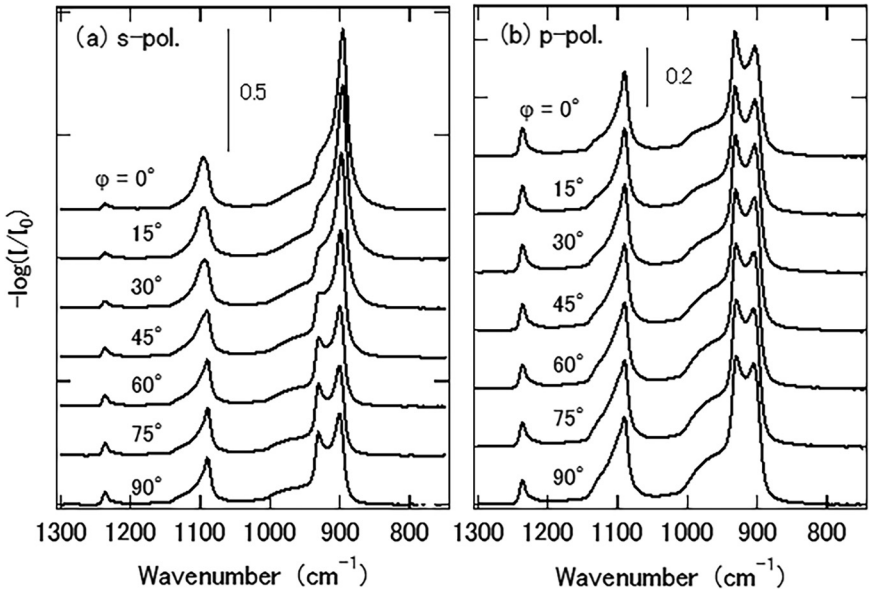

Figure 4. Azimuth angle dependence of the polarized ATR spectra of injection-molded POM: (a) *s*-polarization and (b) *p*-polarization.

phenomena such as peak shifts, shoulder generation (peak asymmetry), and the appearance of new peaks occur in the azimuth angle dependence of Yeh's anisotropic mixing on the ATR spectra (Figures S5–S7, Supplemental Material). Furthermore, when the peak positions of the two modes are close to each other, the above phenomena occur within a narrow frequency range (Figure S8, Supplemental Material). These ATR spectra behaviors are difficult to predict using conventional knowledge based on small-frequency dispersions; thus, they result in the risk of erroneous peak assignments and flawed data interpretation.

Figure 5a shows the azimuthal dependence of the ATR spectrum, calculated using Yeh's equation and the RP of Figure 2 or the CRI of Figure S2 (Supplemental Material). The incident medium was assumed to have a refractive index of four, and the incident angle was set to 45° in Yeh's equation. The vertical axis was plotted on a logarithmic scale that corresponded to the absorption spectrum. A two-phase model was used in the calculation, including the bimodal effect, and the mixing of orthogonal components was set to 17.8% for each azimuth, as in the calculation of reflection. As a result, the shoulder peaks at approximately 1000–950 and 1130–1100 cm^{-1} can be partly explained by considering anisotropy. In particular, the shape of the shoulder peak for *p*-polarization at $\varphi = 90°$ agrees with the experimental data, and the tendency for the shoulder to decrease as the value of φ decreases also matches the experimental data. The generation of these shoulder peaks can also be explained near $\varphi = 45°$ for *s*-polarization. In other words, the anisotropic medium treatment for POM can explain the shoulder peaks when there are vibration modes with large frequency dispersion.

However, there are some discrepancies between the calculated results and the experimental results displayed in Figure 4. The shoulder is not observed in the calculation results for *s*-polarization at $\varphi = 90°$. Moreover, the shoulder shape is not clearly observed in the calculation results for *p*-polarization at $\varphi = 0°$.

The orientation distribution of the main chains in the *z*-direction was not taken into account in our proposed model. If the main chains are distributed in the *z*-direction, the RPs will exhibit differences in the in-plane and depth directions in the *p*-polarized spectrum at $\varphi = 0°$. Therefore, it is possible to obtain spectra with shoulder wings even without considering bimodality. However, it is difficult to explain the shoulder wing in the *s*-polarized spectrum at $\varphi = 90°$, whether by considering the distribution of the main chains in the *z*-direction or including the cross-component in a two-phase model. We tentatively conducted calculations assuming a mixture of cross-components, using the EMT, and the results are shown in Figure 5b. The effective RPs in the direction of injection ($\varepsilon_{c,\mathrm{eff}}$) and in the transverse direction ($\varepsilon_{b,\mathrm{eff}}$) were calculated by mixing the RPs of the main-chain direction (ε_c) and the orthogonal direction (ε_b), using the Bruggeman equation:[31]

$$(1 - f_1)\frac{\varepsilon_c - \varepsilon_{c,\mathrm{eff}}}{\varepsilon_c + 2\varepsilon_{c,\mathrm{eff}}} + f_1\frac{\varepsilon_b - \varepsilon_{c,\mathrm{eff}}}{\varepsilon_b + 2\varepsilon_{c,\mathrm{eff}}} = 0 \qquad (19)$$

$$(1 - f_2)\frac{\varepsilon_b - \varepsilon_{b,\mathrm{eff}}}{\varepsilon_b + 2\varepsilon_{b,\mathrm{eff}}} + f_2\frac{\varepsilon_c - \varepsilon_{b,\mathrm{eff}}}{\varepsilon_c + 2\varepsilon_{b,\mathrm{eff}}} = 0 \qquad (20)$$

where $f_1 = f_2 = 0.178$ for each main-chain and orthogonal RP.

Afterward, the ATR spectrum at each azimuth angle was calculated considering the anisotropic medium by substituting the effective CRI in Eqs. 1–8 and 15–18. In particular, when focusing on the shoulder, these results explain the experimental behaviors shown in Figure 4. Thus, the azimuthal dependence of these ATR spectra can be explained by mixing the cross RPs using the EMT

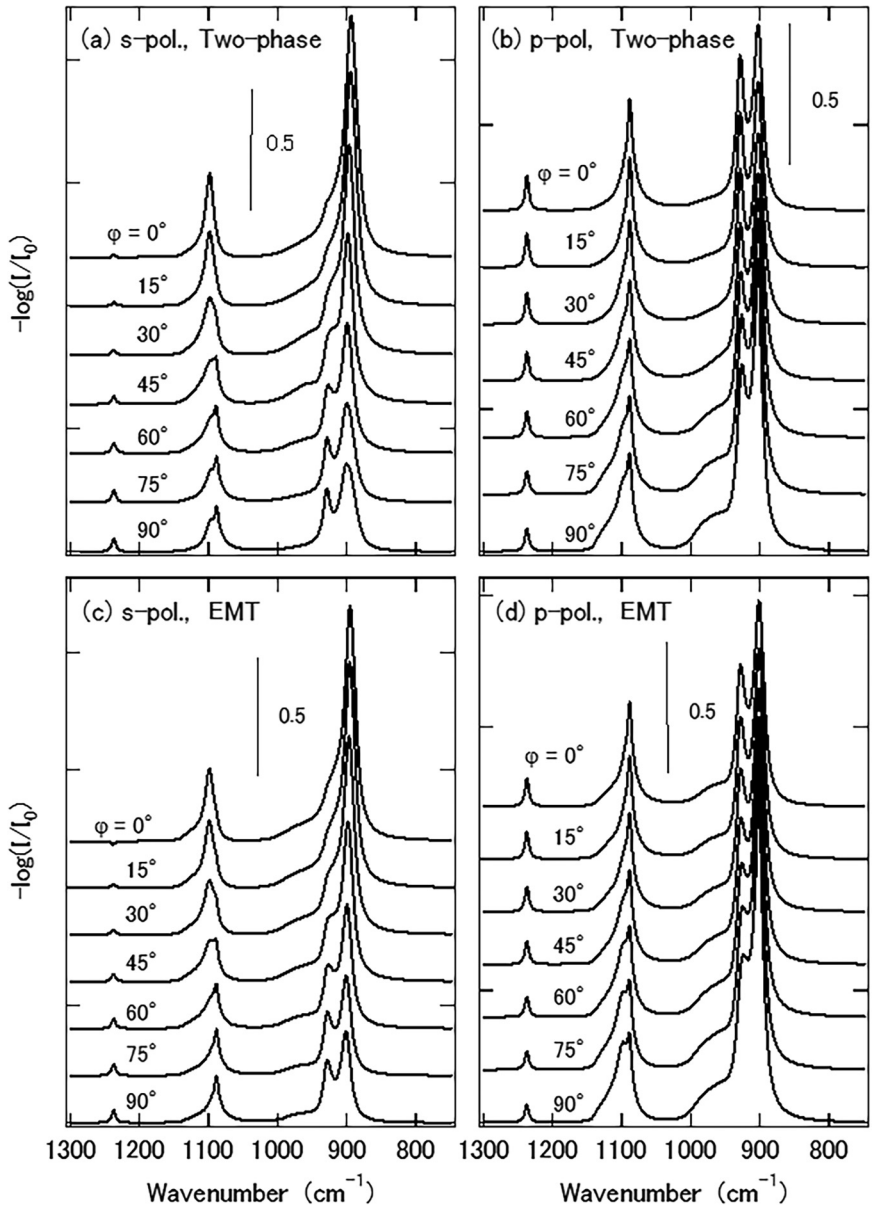

Figure 5. Azimuth angle dependence of the polarization ATR spectra of injection-molded POM calculated using the RP in Figure 2 or the CRI in Figure S2 (Supplemental Material) on the two-phase model: (a) *s*-polarization and (b) *p*-polarization. For the EMT: (c) *s*-polarization and (d) *p*-polarization.

and treating them as anisotropic media, especially regarding the shoulder.

The intensity of the mode at approximately 930–900 cm^{-1} in the calculated spectra seems to be quite different from the experimental results in Figure 4. The difference in the spectra with *p*-polarization is particularly noticeable. This is probably due to the inevitable change in the contact degree between the prism and the sample surface in the ATR measurements. Figure S9 (Supplemental Material) shows the dependence between the gap thickness of the experimental and calculated results of the ATR spectra of POM for *p*-polarization at $\varphi = 90°$. Because it is difficult to control a gap thickness of several tens of nanometers, the ATR spectra were measured by gradually releasing the pressing rod. The calculation was performed using the usual three-layer model shown in the equations below,[32] where the first layer is Ge ($n = 4$), the second layer is air ($n = 1$), and the third layer is an anisotropic POM (Figure S9b, Supplemental Material).

$$r_s = \frac{r_{12,s} + r_{23,ss}e^{-2i\phi}}{1 + r_{12,s}r_{23,ss}e^{-2i\phi}} \tag{21}$$

$$r_p = \frac{r_{12,p} + r_{23,pp}e^{-2i\phi}}{1 + r_{12,p}r_{23,pp}e^{-2i\phi}} \tag{22}$$

$$\phi = \frac{2\pi}{\lambda} n_2 d \cos\theta_2 \quad (23)$$

where r_s and r_p are the reflection coefficients of *s*- and *p*-polarization, r_{12} is the reflection coefficient of the interface of Layer 1 (prism) and Layer 2 (air), and r_{23} is the reflection coefficient of the interface of Layers 2 and 3 (POM), and d is the gap thickness between the prism and the surface of the POM.

There is no mixing term of *s*-polarization and *p*-polarization due to reflection when the azimuth angle is 0° or 90°, but the mixing term of polarization appears when $0° < \varphi < 90°$; in this case, further multiple reflections must be calculated, so the above equation cannot be used. Therefore, these calculations were performed only for azimuth angles of 0° and 90°. The suffix *ss* or *pp* means the components that exclude the polarization conversion term such as r_{ps} or r_{sp} in the reflection at each interface. By comparing the experimental and calculated results, the changes in the spectral shape observed as the ATR pressing rod was released match well with those obtained by increasing the gap thickness in the calculation. The experimental spectra obtained by assuming sufficient contact between the prism and the sample matched well with the calculated spectra with gap thicknesses of approximately 40–100 nm.

We compared the calculation results of the above three-layered model and the EMT with the measured results for *s*-polarized light at $\varphi = 0°$ and 90° and *p*-polarized light at $\varphi = 0°$ and 90°, as shown in Figure 6. All calculations were performed assuming a gap thickness of 60 nm. It appears that, in the case of Figure 6d, the gap used is adequate for the 930–900 cm^{-1} region but not for the 1100 cm^{-1} region. The reason for this is unclear, but there may be morphological effects such as the presence of internal pores, or there may be other reasons such as the presence of *z*-direction orientation components. Overall, the shape of the spectra can be explained by the effective medium anisotropy model, considering the contact with the prism.

Discussion

It is remarkable that the azimuthal dependence of the ATR spectral shapes for both *s*- and *p*-polarized light can be explained by only the RPs calculated using the *s*-polarized reflection spectrum. Yeh's equation is effective in predicting the spectral shape of any azimuthal angle of uniaxial crystals. Because the equation is free of approximations, it can be applied even to polariton bands with large frequency dispersion. Moreover, the equation provides not only R_{ss} (*s*-polarized reflection by *s*-polarized incident light) but also R_{ps} (converted *s*-polarized reflection by *p*-polarized incident light). Figure S10 (Supplemental Material) shows the reflection spectra of *s*- and *p*-polarized light with polarizers inserted only after reflection (R_s and R_p) and R_{ss} and R_{pp} spectra with polarizers inserted not only after but also before reflection for azimuth angles of 0°, 45°, and 90°. For azimuth angles of 0° and 90°, the R_s and R_{ss} and R_p and R_{pp} spectra are almost identical because there is no component converting polarization during reflection in these cases. On the other hand, when the azimuthal angle is 45°, the R_s and R_{ss} (and also R_p and R_{pp}) are not identical and the reflectivity is higher than in the case when no polarizer is inserted on the incident side, indicating that polarization conversion occurs during reflection. Hence, the difference between R_s and R_{ss} results

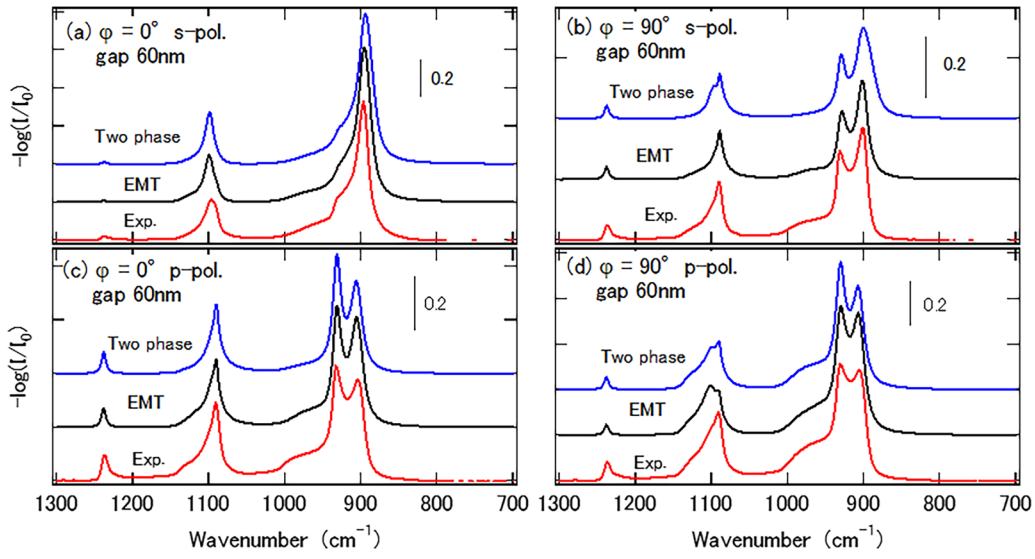

Figure 6. Comparison between the measured polarized ATR spectra of injection-molded POM and the calculated spectra from the RP in Figure 2 or the CRI in Figure S2 (Supplemental Material). Red line: measured spectra. Black line: calculated spectra (EMT). Blue line: calculated spectra (two-phase model): (a) *s*-polarization, $\varphi = 0°$; (b) *s*-polarization, $\varphi = 90°$; (c) *p*-polarization, $\varphi = 0°$; and (d) *p*-polarization, $\varphi = 90°$.

in R_{ps} (and also the difference between R_p and R_{pp} results in R_{sp}). The spectral shape of the results of R_{ps} and R_{sp} calculated using Yeh's equation agrees with the experimental results. This converted reflection appears in the region where the real component of the RP of the main-chain direction is negative. However, the measured R_{ps} and R_{sp} are less than one-third of the calculated values. In other words, the value of the component converted from *p* to *s* (or *s* to *p*) is lower than that of the calculation. The calculated results show a perfectly oriented case in the injection direction. As reported in our previous paper, this material has a nest-like structure whose breadth is approximately 100 nm as revealed by field emission scanning electron microscopy measurements, and the molecules are oriented perpendicular to the thin breadth of the nest.[25] Therefore, components oriented at 45° of the main chain also coexist (i.e., the orientation along the direction of injection is not perfect). Thus, polarization light with a 45° direction should reflect in the same direction of vibration. Namely, this reflection component is not the polarization-converted light because of anisotropy. The contribution of reflection through *s* (or *p*) polarization is added to R_{ss} (or R_{pp}) at $\varphi = 45°$, resulting in lower R_{ps} and R_{sp} components, as shown in the solid lines of Figure S10c and S10d (Supplemental Material). By contrast, the analysis of these R_{ps} and R_{sp} components may be useful for gaining more information on the in-plane orientation structures of the molecules.

Figure S11 (Supplemental Material) displays the *s* and *ss* spectra for the *s*-polarized ATR measurements at azimuth angles of 0°, 45°, and 90°. As previously stated, only the *s*-polarization results are shown because the ATR spectral shape is sensitive to the contact between the sample surface and the prism for *p*-polarization. Hence, when discussing difference spectra, *s*-polarization is more suitable than *p*-polarization. The results for the 0° and 90° azimuth angles exhibit nearly identical shapes in I_s and I_{ss} (Figures S11a and S11c, Supplemental Material), but for the 45° angle (Figure S11b, Supplemental Material), there are regions where the *s* and *ss* spectra are not overlapped. By adjusting the coefficients to subtract the peak at 930 cm^{-1} and calculating the difference spectrum, we obtai Suned the solid-line spectrum in Figure S11d (Supplemental Material). The I_{ps} ($= I_s - I_{ss}$) calculated using Yeh's equation exhibits a similar spectral shape to the measured spectrum, but the band intensity at 900 cm^{-1} is slightly weaker, and the width is somewhat broader compared to the measured spectrum. The I_{ps} spectrum is the component in which the incident light of the *p*-polarization is converted to the *s*-polarization after ATR, and the spectral shape resembles the *s*-polarized spectrum at an azimuth angle of 0°. We anticipate there will be some components in which the main chains are oriented to 45°. ATR spectra generally reflect absorption (the imaginary component of the RP) more prominently than dispersion (the real component of the RP). Therefore, if there is a component that is oriented at 45°, the spectrum corresponding to the imaginary component in Figure 2a is expected to appear during the measurement at $\varphi = 45°$, and this is indeed the case. Therefore, the azimuth angle dependence of ATR can be useful to analyze the orientation state more precisely as well as the reflection. Some discrepancies between the experiments and the calculated results of azimuth angle dependence may be due to orientation imperfections in the actual POM sample.

As an interesting point, the mixing ratio of cross-components in terms of the bimodal characteristics could not be reproduced by the two-phase model in the ATR spectra, even though the ratio could be calculated by applying the two-phase model in the reflection spectra. Calculations of the ATR spectra using EMT could better explain the measured spectra. On the other hand, as previously reported,[25] the reflection spectra could not be explained by the EMT. From a morphological standpoint, the nest's size is small enough compared to the incident wavelength, allowing the application of the EMT. In addition, the composition ratio of the cross-component (17.8%) is also within the applicable range of the EMT.[33]

To investigate the mixing between the main-chain direction and the orthogonal direction, known as the bimodal effect, the mixing of well-defined Lorentz model spectra should be applied. The *s*-polarized reflection and ATR spectra calculated by the two-phase model and the EMT estimated using the two Lorentz models in Figure S3h (Supplemental Material) with the same ratio (17.8%) are shown in Figure S12 (Supplemental Material). These Lorentzian models can produce POM-like spectra. In the reflection spectrum, when incorporating the bimodal effect with the two-phase model, a substantial frequency dispersion remains at approximately 1000 cm^{-1} as a Reststrahlen band, even in the 17.8% mixing of a larger Lorentzian dispersion. However, in the ATR spectrum of the two-phase model, the strong absorption is reflected in the mixing results in a shape that simply adds two Lorentz peaks. This result deviates from the experimental data. On the other hand, by applying the EMT, the substantial frequency dispersion is diluted, making the Reststrahlen band less prominent in the reflection spectrum. However, instead of a simple addition of Lorentz peaks, the ATR spectrum still reflects the influence of frequency dispersion, resulting in a spectrum that is closer to the experimental data. These results suggest that spectra that reflect frequency dispersion appear in both the reflection and ATR measurements.

The selection of the model should be judged by the experiments. When the absorption and the frequency dispersion are small, the mixed spectrum may be reproduced by either model. However, in the case of a large dispersion, differences among the chosen models can be detected. In our experiments, there is a difference between the analysis probe of the reflection spectrum using ordinary light (far-field light) and the ATR analysis probe using evanescent waves (near-field light). Thus, the selection of the model may be affected by the physical dispersion state or morphology depending on the probe. It is currently unclear why a single model cannot explain both the reflectance and ATR spectra of POM.

Although there are still discrepancies between the calculations and the results from the reflection and ATR experiments in this study, it might be necessary to evaluate the spectra using more accurate RPs. Despite the existence of a few hundred nanometer-sized voids on the POM surface, the arguments presented above were based on the RPs obtained using the reflection spectra. Therefore, these RPs already incorporated the effects of morphology (the mean values of POM and air). Moreover, the reflection is extremely sensitive to external perturbations such as pressing and rubbing, which affect the spectral shapes.[22] This means that the surface polariton effects are included in the determination of the RPs. Ideally, the RP should be determined considering the void fraction. Such an RP would likely have a larger intensity and dispersion than the RPs shown here. Furthermore, such RPs would enable us to calculate the influence of morphology at the same time, making it possible to construct a single model capable of interpreting both the reflection and ATR spectra while incorporating the frequency dispersion.

The orientation distribution of the main chains in the z-direction is not considered in the proposed model. By considering the distribution of the main chains in the z-direction and the various factors mentioned above carefully, it may be possible to interpret the orientation-dependent spectra with a single model. However, the evaluation processes described above are expected to be challenging and require further research.

Conclusion

We calculated the azimuthal dependence of reflection and ATR spectra based on the consistent determination of the RPs for the main-chain and orthogonal directions from the s-polarized reflection spectra. POM has a strong absorption and large frequency dispersion in the main-chain direction and Reststrahlen bands are observed in the reflection. We found that the azimuthal dependence of this shape can be explained by Yeh's equation, considering the polarization conversion components of R_{ps} and R_{sp}. In the ATR spectra, phenomena such as the appearance of new shoulder wings occur, but these can be understood by the calculation of the azimuth angle dependence, using Yeh's equation. The peak shifts and presence of new apparent peaks due to anisotropic mixing are crucial phenomena to be aware of to avoid misinterpretations. Injection-molded POM exhibits a bimodal main-chain orientation; thus, a choice can be made whether a two-phase model or EMT is used during mixing. The shape of the spectrum can be explained by the two-phase model in terms of reflection and EMT for ATR in addition to optical anisotropy. Moreover, the applicable model differs depending on the analysis probe even in the same IR region.

Declaration of Conflicting Interests

The author declared no potential conflicts of interest with respect to the research, authorship, and/or publication of this article.

Funding

The author received no financial support for the research, authorship, and/or publication of this article.

ORCID iD

Naoto Nagai https://orcid.org/0000-0002-0176-7954

Supplemental Material

All supplemental material mentioned in the text is available in the online version of the journal.

Appendix

Azimuth angle dependence of ATR spectra using anisotropic Lorentz bands with various frequency dispersions.

Figure S3 (Supplemental Material) shows Lorentzian-type RPs with peaks at 1100 cm^{-1} with different frequency dispersions in Figures S3a–S3d (Supplemental Material) and RPs with a peak at 950 cm^{-1} in Figures S3e–S3g (Supplemental Material). Figure S3h (Supplemental Material) shows two RPs with close peak positions of 900 and 930 cm^{-1} but with substantially different frequency dispersions. These spectra are represented by the following Lorentzian equation, and each parameter is summarized in Table S1 (Supplemental Material).

$$\varepsilon_r(\nu) = \varepsilon_{r,\infty} + \frac{\Omega_p^2}{\Omega^2 - \nu^2 - i\nu\gamma} \tag{24}$$

here, we took $\epsilon_{r,\infty} = 2.3$ (typical RP of polymers) for the Lorentzian peak calculations.

In Figures S3d and S3g (Supplemental Material), the imaginary component of the RP is above 20, which is larger than that for POM in Figure 2. While such cases are possible in inorganic ionic crystals, they seem unlikely in polymers. However, it is worth noting that, in the case of POM, even when heated slightly below its melting point, values well above 40 for the imaginary component of the RP can occur.[25] Moreover, in extrusion molding, this value can exceed 70 in some cases.[23] Therefore, in highly polar and crystalline polymers, such situations can occur through various mechanical or thermal processes.

Figure S4 (Supplemental Material) shows the azimuthal dependence of ATR spectra, according to Yeh's equation, for a uniaxial crystal corresponding to the RP of the *c*-axis in Figure S3e (Supplemental Material) and those of the *a*- and *b*-axes in Figure S3a (Supplemental Material). The azimuthal dependence shown in this Appendix was represented as ATR spectra, using a Ge prism with a refractive index of four and an incident angle of 45°. The results in Figure S4 (Supplemental Material) correspond to normal polymers with relatively small-frequency dispersion. In this case, the spectra for $0° < \varphi < 90°$ become just a mixture of the 1100 cm^{-1} peak and the 950 cm^{-1} peak. The shape of the spectrum for the *p*-polarization at $\varphi = 90°$ also appears to be simply the mixture of each mode, indicating the occurrence of the anisotropy effect.

Figure S5 (Supplemental Material) shows the azimuthal dependence of ATR spectra for a uniaxial crystal corresponding to the RP of the *c*-axis in Figure S3g (Supplemental Material) and those of the *a*- and *b*-axes in Figure S3b (Supplemental Material). The spectrum for the 950 cm^{-1} mode with a larger frequency dispersion exhibits substantial changes in spectral width, peak position, and a shoulder on the high-frequency side depending on the azimuth angle, unlike the case in Figure S4 (Supplemental Material), and does not appear to be a simple mixing.

Figure S6 (Supplemental Material) shows the azimuthal dependence of the ATR spectrum for a uniaxial crystal with the RP of the *c*-axis in Figure S3f (Supplemental Material) and those of the *a*- and *b*-axes in Figure S3c (Supplemental Material), respectively. Although the peak positions are separated by approximately 150 cm^{-1}, both modes are negative in the real component of the RP. In this case, the peak shifts and the appearance of the shoulders depend on the azimuth angle.

Figure S7 (Supplemental Material) shows the azimuthal dependence of the ATR spectrum for a uniaxial crystal with the RP of the *c*-axis in Figure S3g (Supplemental Material) and those of the *a*- and *b*-axes in Figure S3d (Supplemental Material). Both modes have a large frequency dispersion and a large negative real component of the RP. Phenomena such as peak shifts, changes in half-width, and appearance of shoulders are observed as well as the emergence of new peaks near 1170 cm^{-1} in the *s*-polarized spectra at $\varphi = 30°$ and 45°. Notwithstanding, these spectra are composed of only two vibrational modes.

Figure S8 (Supplemental Material) is a case where two modes (a 900 cm^{-1} peak along the *c*-axis and a 930 cm^{-1} peak along the *a*- and *b*-axes in Figure S3h, Supplemental Material) are separated by only 30 cm^{-1} and the real component of the RP of the 900 cm^{-1} mode becomes negative (a case close to POM anisotropy). Even in this case, a drastic azimuthal dependence is evidenced by changes in the peak width, shift, and shoulder occurrence.

In all of the above cases, polarized ATR spectra exhibit shoulders or other apparent peak deformations depending on the azimuth angle when there is a mode with a large frequency dispersion existing along one or two crystal axes. These phenomena occur due to the mixing of the two RPs in anisotropic media, and caution is required in interpreting the spectra, as they may appear to have three or more modes, especially when measured with unpolarized light.

As a preliminary finding, in optical anisotropy, mixing between peaks with a relatively large dispersion in the real part of RP (without becoming negative, e.g., Figure 3b) and peaks with a small dispersion (e.g., Figure 3e) results in peak shifts only when changing the azimuth angle.

References

1. H. Tadokoro, S. Yasumoto, S. Murahashi, I. Nitta. "Molecular Configuration of Polyoxymethylene". J. Polym. Sci. 1960. 44 (143): 266–269.
2. G. Carazzolo. "Structure of the Normal Crystal Form of Polyoxymethylene". J. Polym. Sci., Part A. 1963. 1(5): 1573–1583.
3. L. Terlemezyan, M. Mihailov, P. Schmidt. "Conformational Changes of Poly(Oxymethylene) Induced by Pressure and Mechanical Treatment". Makromol. Chem. 1978. 179(3): 807–813.
4. L. Terlemezyan, M. Mihailov, P. Schmidt, B. Schneider. "Temperature Changes of Poly(Oxymethylene) Structures Studied by Infrared Spectroscopy". Makromol. Chem. 1978. 179(9): 2315–2322.
5. L. Terlemezyan, M. Mihailov. "Dependence of the Conformation of Nascent Poly(Oxymethylene) on the Conditions of Cationic Polymer: Cation of Trioxane in Solution". Eur. Polym. J. 1981. 17 (11): 1115–1120.
6. E.F. Oleinik, N.S. Enikolopyan. "Conformations and Molecular Structure of the Chains with $(C–O)_n$ Backbone". J. Polym. Sci. Part C. 1967. 16(7): 3677–3683.
7. V. Zamboni, G. Zerbi. "Vibrational Spectrum of a New Crystalline Modification of Polyoxymethylene". J. Polym. Sci. Part C. 1964. 7(1): 153–161.
8. G. Carazzolo, M. Mammi. "Crystal Structure of a New Form of Polyoxymethylene". J. Polymer. Sci. Part A. 1963. 1(3): 965–983.
9. M. Iguchi. "Growth of Needle-Like Crystals of Polyoxymethylene During Polymerization". Br. Poly. J. 1973. 5(3): 195–198.
10. M. Iguchi, M. Murase. "Polymorphosis of Poly(Oxymethylene) Crystals Grown in a Cationic Polymerization System of 1,3,5-Trioxane in Solution". Makromol. Chem. 1975. 176(7): 2113–2126.
11. M. Iguchi, I. Murase. "Growth of Needle-Like Polyoxymethylene Crystals". J. Crystal. Growth. 1974. 24–25: 596–599.
12. M. Kobayashi, M. Sakashita. "Morphology Dependent Anomalous Frequency Shifts of Infrared Absorption Bands of Polymer Crystals: Interpretation in Terms of Transition Dipole–Dipole Coupling Theory". J. Chem. Phys. 1992. 96(1): 748–760.
13. Y. Tanabe, M. Shimomura. "A_2 Mode Vibrations in Infrared Absorption Spectrum of Trigonal Poly(Oxymethylene)". Macromolecules. 1990. 23(23): 5031–5034.
14. M. Tashiro, G. Wu, M. Kobayashi. "Morphological Effect on the Raman Frequency Shift Induced by Tensile Stress Applied to Crystalline Polyoxymethylene and Polyethylene: Spectroscopic Support for the Idea of an Inhomogeneous Stress Distribution in Polymer Material". Polymer. 1988. 29(10): 1768–1778.
15. H. Hama, K. Tashiro. "Structural Changes in Non-Isothermal Crystallization Process of Melt-Cooled Polyoxymethylene. [I] Detection of Infrared Bands Characteristic of Folded and Extended Chain Crystal Morphologies and Extraction of a Lamellar Stacking Model". Polymer. 2003. 44(10): 3107–3116.
16. H. Hama, K. Tashiro. "Structural Changes in Non-Isothermal Crystallization Process of Melt-Cooled Polyoxymethylene [II] Evolution of Lamellar Stacking Structure Derived from SAXS and WAXS Data Analysis". Polymer. 2003. 44(7): 2159–2168.
17. H. Hama, K. Tashiro. "Structural Changes in Isothermal Crystallization Process of Polyoxymethylene Investigated by Time-Resolved FTIR, SAXS, and WAXS Measurements". Polymer. 2003. 44(22): 6973–6988.
18. M. Shimomura, M. Iguchi, M. Kobayashi. "Vibrational Spectroscopic Study on Trigonal Polyoxymethylene and Polyoxymethylene-d_2 Crystals". Polymer. 1988. 29(2): 351–357.
19. M. Kobayashi, H. Morishita, M. Shimomura. "Pressure-Induced Phase Transition of Poly(Oxymethylene) from the Trigonal to the Orthorhombic Phase: Effect of Morphological Structure". Macromolecules. 1989. 22(9): 3726–3730.

20. A.W. Laramée, C. Lanthier, C. Pellerin. "Electrospinning of Highly Crystalline Polymers for Strongly Oriented Fibers". Appl. Polym. Mater. 2020. 2(11): 5025–5032.
21. H. Miyaji. "Hydrostatic Compression of Polyoxymethylene". J. Phys. Soc. Japan. 1975. 39: 1346–1350.
22. N. Nagai, M. Okawara, Y. Kijima. "Infrared Response of Sub-Micron-Scale Structures of Polyoxymethylene: Surface Polaritons in Polymers". Appl. Spectrosc. 2016. 70(8): 1278–1291.
23. N. Nagai, H. Okada, Y. Amaki, M. Okamura, et al. "Anomalous High-Infrared Reflectance of Extruded Polyoxymethylene". AIP Advances. 2020. 10(9): 095201.
24. N. Nagai, H. Okada, T. Hasegawa. "Morphology-Sensitive Infrared Absorption Bands of Polymers Derived from Surface Polaritons". AIP Advances. 2019. 9(10): 105203.
25. Y. Amaki, H. Okada, N. Nagai. "Structural Analysis of Injection-Molded Polyoxymethylene Treated Below a Melting Point Using Field-Emission Scanning Electron Microscopy and Infrared Spectroscopy". Appl. Spectrosc. 2022. 76(6): 699–711.
26. J.P. Devlin, G. Pollard, R. Frech. "ATR Infrared Spectra of Uniaxial Nitrate Crystals". J. Chem. Phys. 1970. 53(11): 4147–4151.
27. P. Koziol, D. Liberda, W.M. Kwiatek, T.P. Wrobel. "Macromolecular Orientation in Biological Tissues Using a Four-Polarization Method in FT-IR Imaging". Anal. Chem. 2020. 92(19): 13313–13318.
28. M. Makarem, C.M. Lee, K. Kafle, S. Huang, et al. "Probing Cellulose Structures with Vibrational Spectroscopy". Cellulose. 2019. 26: 35–79.
29. C.Z. Tan, H. Li, I. Chen. "Generation of Mutual Coherence of Eigenvibrations in α-Quartz at Infrared Frequencies by Incidence of Randomly Polarized Waves". Appl. Phys. B. 2007. 86: 129–137.
30. P. Yeh. "Optics of Anisotropic Layered Media". In: Optical Waves in Layered Media. Hoboken, New Jersey: John Wiley and Sons, Inc., 1998. Chap. 9. Pp. 201–253.
31. D.A.G. Bruggeman. "Berechnung Verschiedener Physikalischer Konstanten von Heterogenen Substanzen. I. Dielektrizitätskonstanten und Leitfähigkeiten der Mischkörper aus Isotropen Substanzen". Ann. Phys. 1935. 416(7): 636–664.
32. P. Yeh. "Optics of A Single Homogeneous and Isotropic Layer". In: Optical Waves in Layered Media. Hoboken, New Jersey: John Wiley and Sons, Inc., 1998. Chap. 4. Pp. 83–101.
33. T.C. Choy. "Essentials". In: Effective Medium Theory: Principles and Applications. Oxford: Oxford University Press, 2016. Chap. 1. Pp. 1–26.